

University of Groningen

## Functional and Structural Characterization of an Unusual Cofactor-Independent Oxygenase

Baas, Bert-Jan; Poddar, Harshwardhan; Geertsema, Edzard M; Rozeboom, Henriette J; de Vries, Marcel; Permentier, Hjalmar P; Thunnissen, Andy-Mark W H; Poelarends, Gerrit J

*Published in:*  
Biochemistry

*DOI:*  
[10.1021/bi501200j](https://doi.org/10.1021/bi501200j)

**IMPORTANT NOTE:** You are advised to consult the publisher's version (publisher's PDF) if you wish to cite from it. Please check the document version below.

*Document Version*  
Publisher's PDF, also known as Version of record

*Publication date:*  
2015

[Link to publication in University of Groningen/UMCG research database](#)

*Citation for published version (APA):*

Baas, B.-J., Poddar, H., Geertsema, E. M., Rozeboom, H. J., de Vries, M., Permentier, H. P., Thunnissen, A.-M. W. H., & Poelarends, G. J. (2015). Functional and Structural Characterization of an Unusual Cofactor-Independent Oxygenase. *Biochemistry*, 54(5), 1219-1232. <https://doi.org/10.1021/bi501200j>

### Copyright

Other than for strictly personal use, it is not permitted to download or to forward/distribute the text or part of it without the consent of the author(s) and/or copyright holder(s), unless the work is under an open content license (like Creative Commons).

The publication may also be distributed here under the terms of Article 25fa of the Dutch Copyright Act, indicated by the "Taverne" license. More information can be found on the University of Groningen website: <https://www.rug.nl/library/open-access/self-archiving-pure/taverne-amendment>.

### Take-down policy

If you believe that this document breaches copyright please contact us providing details, and we will remove access to the work immediately and investigate your claim.

*Downloaded from the University of Groningen/UMCG research database (Pure): <http://www.rug.nl/research/portal>. For technical reasons the number of authors shown on this cover page is limited to 10 maximum.*

# Functional and Structural Characterization of an Unusual Cofactor-Independent Oxygenase

Bert-Jan Baas,<sup>†</sup> Harshwardhan Poddar,<sup>†</sup> Edzard M. Geertsema,<sup>†</sup> Henriette J. Rozeboom,<sup>§</sup> Marcel P. de Vries,<sup>‡,||</sup> Hjalmar P. Permentier,<sup>‡</sup> Andy-Mark W.H. Thunnissen,<sup>§</sup> and Gerrit J. Poelarends<sup>\*,†</sup>

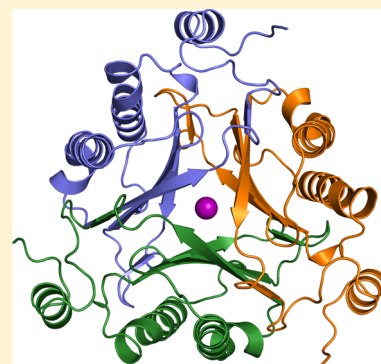
<sup>†</sup>Department of Pharmaceutical Biology, Groningen Research Institute of Pharmacy and <sup>‡</sup>Analytical Biochemistry and Mass Spectrometry Core Facility, Department of Pharmacy, University of Groningen, Antonius Deusinglaan 1, 9713 AV Groningen, The Netherlands

<sup>§</sup>Department of Biophysical Chemistry, Groningen Biomolecular Sciences and Biotechnology Institute, University of Groningen, Nijenborgh 7, 9747 AG Groningen, The Netherlands

<sup>||</sup>Department of Pediatrics, University Medical Center Groningen, University of Groningen, Hanzeplein 1, 9713 GZ Groningen, The Netherlands

## S Supporting Information

**ABSTRACT:** The vast majority of characterized oxygenases use bound cofactors to activate molecular oxygen to carry out oxidation chemistry. Here, we show that an enzyme of unknown activity, RhCC from *Rhodococcus jostii* RHA1, functions as an oxygenase, using 4-hydroxyphenylenolpyruvate as a substrate. This unique and complex reaction yields 3-hydroxy-3-(4-hydroxyphenyl)-pyruvate, 4-hydroxybenzaldehyde, and oxalic acid as major products. Incubations with H<sub>2</sub><sup>18</sup>O, <sup>18</sup>O<sub>2</sub>, and a substrate analogue suggest that this enzymatic oxygenation reaction likely involves a peroxide anion intermediate. Analysis of sequence similarity and the crystal structure of RhCC (solved at 1.78 Å resolution) reveal that this enzyme belongs to the tautomerase superfamily. Members of this superfamily typically catalyze tautomerization, dehalogenation, or decarboxylation reactions rather than oxygenation reactions. The structure shows the absence of cofactors, establishing RhCC as a rare example of a redox-metal- and coenzyme-free oxygenase. This sets the stage to study the mechanistic details of cofactor-independent oxygen activation in the unusual context of the tautomerase superfamily.



The oxygen-rich environment of the earth's biosphere has provided nature with the opportunity to evolve a vast number of enzymes that have the ability to utilize the strong oxidizing power of molecular oxygen (dioxygen, O<sub>2</sub>).<sup>1,2</sup> These enzymes possess the capacity to activate molecular oxygen in order to oxidize organic substrates. To achieve this, oxidases and oxygenases are dependent on redox cofactors, such as flavin or pterin, or coordinated transition metals, such as Fe<sup>2+</sup> or Cu<sup>+</sup>.<sup>3</sup> In recent years, however, a few O<sub>2</sub>-utilizing enzymes have been discovered that stand apart from classical oxidases and oxygenases because they possess the remarkable ability to activate molecular oxygen without any cofactor, which is a highly unusual property that has evoked great scientific interest.<sup>4</sup>

Cofactor-independent oxidases and oxygenases appear to catalyze a direct reaction between molecular oxygen and an organic substrate, which is both thermodynamically unfavorable as well as chemically forbidden.<sup>2–4</sup> This is because molecular oxygen, in its ground state, exists as a triplet biradical, meaning that its electronic structure has two unpaired electrons in its highest occupied molecular orbitals.<sup>3–5</sup> This results in a total spin quantum number of S = 1 (triplet state), whereas the electronic structure of organic substrates is composed entirely of paired electrons and hence has a spin number of S = 0

(singlet state).<sup>3–5</sup> The direct reaction of a triplet-state molecule with a molecule in the singlet state is spin-forbidden because it violates the Wigner rule of spin conservation.<sup>6</sup> Therefore, standard two-electron reaction mechanisms that are generally valid for reactions involving singlet-state molecules do not apply to molecular oxygen. Cofactors can help enzymes to overcome this barrier by providing spin-allowed reaction mechanisms.<sup>3,5</sup> Activated oxygen species are generated, and the reaction of these with organic substrates is thermodynamically favorable, providing the driving force for these reactions.

Cofactor-independent oxidases and oxygenases must therefore rely on a different mechanism in order to gain access to the oxidizing power of molecular oxygen. Evidence for common mechanistic features is slowly emerging and involves the base-catalyzed formation of a substrate anion and a phenomenon termed substrate-assisted catalysis.<sup>7–10</sup> The anionic form of the substrate is able to reduce molecular oxygen via single-electron transfer, converting it into its superoxide anion form (O<sub>2</sub><sup>•-</sup>). The one-electron-oxidized substrate anion now exists in the

Received: September 24, 2014

Revised: December 17, 2014

Published: January 7, 2015

form of a radical cation; a determining feature of this is the stabilization of the remaining unpaired electron by the electronic structure of the substrate itself. Although the few cofactor-independent oxidases and oxygenases that have been identified to date seem to share mechanistic features, they appear to be unrelated in sequence or structure because they belong to distinct enzyme (super)families.<sup>4</sup> The identification of novel cofactor-independent oxidases or oxygenases from different protein superfamilies as well as the characterization of the structural and mechanistic features that underlie catalysis would provide valuable insights into the mechanistic requirements for cofactor-independent activation of molecular oxygen.

In this work, we report that an enzyme of unknown activity, RhCC from *Rhodococcus jostii* RHA1, functions as a unique cofactor-independent oxygenase that utilizes 4-hydroxyphenyl-enolpyruvate (4HPP) as a substrate. This complex enzymatic reaction likely involves a peroxide anion intermediate and yields 3-hydroxy-3-(4-hydroxyphenyl)-pyruvate, 4-hydroxybenzaldehyde, and oxalic acid as major products. Sequence and structure comparisons demonstrate that this enzyme belongs to the tautomerase superfamily, the members of which are characterized by a structural  $\beta$ - $\alpha$ - $\beta$  fold and a catalytic amino-terminal proline.<sup>11–13</sup> RhCC is the first oxygenase identified within this superfamily, providing a framework to investigate cofactor-independent oxygenation within a structural fold that is generally employed to catalyze tautomerization, dehalogenation, or decarboxylation reactions.

## ■ EXPERIMENTAL PROCEDURES

**Materials.** The sources of the components of buffers and media, PCR purification, gel extraction and miniprep kits, prepacked PD-10 Sephadex G-25 columns, and the oligonucleotides, enzymes, and reagents used in the molecular biology procedures are reported elsewhere.<sup>14</sup> All other chemicals and biochemicals, including 4HPP and phenylenolpyruvate (**9**), were purchased from Sigma-Aldrich Chemical Co. (St. Louis, MO) unless stated otherwise. (*E*)-2-fluoro-*p*-hydroxycinnamic acid (**10**) was a kind gift from Prof. Christian P. Whitman (University of Texas, Austin, TX). The genomic DNA of *R. jostii* RHA1 (GenBank sequence CP000431) was kindly supplied by Dr. Robert van der Geize (University of Groningen, The Netherlands).

**General Methods.** Techniques for restriction enzyme digestions, ligation, transformation, and other standard molecular biology manipulations were based on methods described elsewhere or as suggested by the manufacturer.<sup>15</sup> PCR was carried out in a DNA thermal cycler (model GS-1) obtained from Biogio (Nijmegen, The Netherlands). DNA sequencing was carried out by ServiceXS (Leiden, The Netherlands) or Macrogen (Seoul, Korea). Protein was analyzed by sodium-dodecyl-sulfate–polyacrylamide-gel electrophoresis (SDS-PAGE) in gels containing 10% polyacrylamide. The gels were stained with Coomassie brilliant blue. Protein concentrations were determined by the method of Waddell.<sup>16</sup> Kinetic data were obtained on a V-660 spectrophotometer from Jasco (IJsselstein, The Netherlands). The kinetic data were fitted by nonlinear regression data analysis using the Grafit program (Erithacus, Software Ltd., Horley, U.K.) obtained from Sigma Chemical Co. Protein ESI-MS spectra were recorded using a Sciex API 3000 triple quadrupole mass spectrometer (AB Sciex, Concord, Ontario, Canada). <sup>1</sup>H NMR spectra were recorded on a Bruker DRX-500 (500 MHz) spectrometer. Chemical shifts for protons are reported in parts

per million scale ( $\delta$  scale) and are referenced to H<sub>2</sub>O ( $\delta$  = 4.80). <sup>13</sup>C NMR, COSY, <sup>1</sup>H,<sup>13</sup>C-HSQC, and <sup>1</sup>H,<sup>13</sup>C-HMBC spectra were recorded (CryoNMR) using a Bruker 500 MHz Avance III system (Bruker Biospin, Rheinstetten, Germany). Dynamic light scattering (DLS) experiments were carried out using a DynaPro MS800TC instrument (Wyatt Technology Corporation, Santa Barbara, CA) at 20 °C. DLS data were processed and analyzed with the Dynamics software (Wyatt Technology Corporation).

**Cloning of the Gene Encoding RhCC.** The gene encoding RhCC was amplified via PCR, using two synthetic primers, genomic DNA of *R. jostii* RHA1, and the PCR reagents supplied in the Phusion DNA Polymerase system. The forward primer (5'-A TAG CAG GTA CAT ATG CCG TAC TGG GAG ATC TTC ACG CCC-3') contains an *Nde*I restriction site (bold) that is followed by 24 bases corresponding to the coding sequence of the gene. To clone the gene encoding RhCC in frame with the sequence that codes for the polyhistidine region of the expression vector (pET20b(+)), we used a reverse primer (5'-G TGA TGT TAT AAG CTT CGA GGC AGC GAC GTC GTA CGG A-3') that contains a *Hind*III restriction site (bold). The amplification reaction mixture was made in Phusion High-Fidelity buffer and contained 250  $\mu$ M each dNTP, 150 ng of each primer, 250 ng of genomic DNA, and 1 U of Phusion DNA polymerase. The cycling parameters were as follows: 95 °C for 5 min, then 35 cycles at 98 °C for 30 s, 45 °C for 30 s, and 72 °C for 20 s, and a final elongation step of 72 °C for 10 min. The resulting PCR product and the vector (pET-20b(+), Novagen) were digested with *Nde*I and *Hind*III restriction enzymes, after which the vector was dephosphorylated with alkaline phosphatase. Following purification, the PCR product and vector were ligated using T4 DNA ligase. An aliquot of the ligation mixture was transformed into competent *Escherichia coli* BL21 (DE3) cells. Transformants were selected at 37 °C on LB/ampicillin plates. Plasmid DNA was isolated from several colonies and analyzed by restriction analysis for the presence of the insert. The cloned gene was sequenced to verify that no mutations had been introduced during the amplification of the gene. The newly constructed expression vector was named pRhCC.

**Expression and Purification of RhCC.** The RhCC protein was produced constitutively in *E. coli* BL21 (DE3) using the T7 expression system. Fresh BL21 (DE3) transformants that contained vector pRhCC were collected from an LB/ampicillin plate and used to inoculate a preculture (LB/ampicillin medium, 5 mL). After growth for 3–5 h at 37 °C, the preculture was used to inoculate 1 L of autoinduction (ZYM) medium (10 g/L tryptone, 5 g/L yeast extract, 25 mM Na<sub>2</sub>HPO<sub>4</sub>, 25 mM KH<sub>2</sub>PO<sub>4</sub>, 5 mM Na<sub>2</sub>SO<sub>4</sub> (pH 6.7), supplemented with 0.5% (v/v) glycerol, 0.05% (w/v) glucose, MgSO<sub>4</sub> (2 mM), ampicillin (100  $\mu$ g/mL), and 0.2% (w/v) lactose) in a 3 L Erlenmeyer flask to a starting OD<sub>600</sub> of about 0.01. After overnight growth at 30 °C with vigorous shaking, the cells were harvested by centrifugation (10 min at 2300 g) and resuspended in 10 mM NaH<sub>2</sub>PO<sub>4</sub> buffer (pH 7.3, buffer A) to a total volume of about 10 mL. Protease inhibitors (Complete Mini, Roche, Mannheim, Germany) were added, and the cells were disrupted by sonication (5  $\times$  1 min, with 5 min rest in between each cycle) at 50% duty cycle/50% output in a Branson Sonifier 450 (Branson Ultrasonics Corporation, Danbury, CT). Unbroken cells and debris were removed by centrifugation (45 min at 18 000 g). The supernatant was filtered through a 0.2  $\mu$ m pore diameter filter, diluted to 10 mM

in imidazole (using a 1 M stock solution in water with the pH adjusted to 7.3), and applied to a gravity-flow column containing 0.5 mL of Ni-Sepharose 6 Fast Flow resin. After overnight incubation at 4 °C while mixing at 20 rpm on a rotor, the nonbound proteins were removed from the column by gravity flow. The column was washed with 20 mM imidazole in buffer A and then in 40 mM imidazole in buffer A, after which the retained protein was eluted with 1 mL of 250 mM imidazole in buffer A. Subsequently, the protein solution was applied to a PD-10 gel-filtration column, which was previously equilibrated in buffer A, and proteins were eluted with buffer A. Fractions (1 mL each) were analyzed by SDS-PAGE, and those containing highly purified RhCC were combined and concentrated to a protein concentration of 5–20 mg/mL using a Vivaspin centrifugal concentrator equipped with a 5000 Da molecular weight cutoff filtration membrane (Sartorius Stedim Biotech S.A., France).

**Crystallization of RhCC.** Initial crystallization conditions were determined by vapor-diffusion sitting-drop experiments in MRC 96-well crystallization plates (Molecular Dimensions), using a Mosquito crystallization robot (TTP Labtech) for automatic drop-dispensing. Protein drops were prepared by mixing 200 nL of protein solution (12.5 mg/mL in 20 mM Tris/HCl buffer, pH 7.5) with an equal volume of precipitant reservoir solution. Reservoir solutions were obtained from various commercial crystallization screens, and equilibration was carried out at room temperature. The crystallization lead thus determined was reproduced and optimized manually by vapor-diffusion hanging-drop experiments (drops containing 2  $\mu$ L of protein solution and 2  $\mu$ L of reservoir solution), resulting in the following final crystallization conditions: 5–12.5 mg/mL protein, 24–28% (w/v) polyethylene glycol 3350 (PEG 3350), and 100 mM Bis-Tris-propane (pH 8.0–8.5). Crystals grew within 1 week to an average size of 200  $\times$  100  $\times$  50  $\mu$ m<sup>3</sup>.

**Data Collection, Processing, and Determination of RhCC Structure.** Prior to the collection of X-ray-diffraction data, crystals were soaked briefly in a cryoprotectant solution containing 30% PEG 3350 and 15% glycerol in 100 mM Bis-Tris-propane (pH 8) and subsequently flash-cooled in liquid nitrogen. A 1.78 Å data set was collected at beamline ID14-4 at the European Synchrotron Radiation Facility (Grenoble, France). Diffraction data were processed, scaled, and merged using the programs iMosflm and Aimless from the CCP4 software suite.<sup>17–19</sup> Crystals belonged to space group C22<sub>1</sub> and contained a protein trimer in the asymmetric unit (solvent content = 47%). A summary of the data collection statistics is given in the Supporting Information (Table S). Initial phases were calculated by the molecular replacement method with the help of the program Phaser.<sup>20</sup> The unpublished structure of AU4130/APC7354, a putative tautomerase from the thermophilic fungus *Aspergillus fumigatus* (Protein Data Bank (PDB) entry 3C6V), served as molecular replacement search model. The RhCC structure was improved and completed by iterative cycles of refinement in Refmac5, alternated by manual model building in Coot. The final cycles of refinement were carried out using the program phenix.refine from the Phenix software suite.<sup>21</sup> At the early stages of model building, a bound metal ion was identified at the surface of the RhCC trimer, positioned at the noncrystallographic 3-fold symmetry axis. Based on the metal-coordination geometry, the absence of anomalous difference electron density, and analysis of the B factors in the later stages of refinement, the bound metal was identified as a Mg<sup>2+</sup> ion.

**Construction of the D106A Mutant.** The D106A variant of RhCC was constructed by overlap-extension PCR, using the Phusion DNA polymerase system. Synthetic primers 5'-G GAG ATC CAC ATC GCC GAG ACC CCC ATG GAC C-3' and 5'-G GTC CAT GGG GGT CTC GGC GAT GTG GAT CTC C-3' were used to introduce the desired mutation (underlined). These primers were used in combination with the general T7-forward and T7-reverse primers of the pET system. The mutant gene was cloned into the expression vector (pET-20b(+)) as described above for the wild-type gene. The cloned gene was sequenced to verify that only the desired mutation was introduced.

**Purification, Crystallization, and Determination of the D106A Mutant Protein Structure.** The D106A mutant protein was produced and purified following procedures identical to those used for wild-type RhCC, except that the cells were grown in autoinduction medium at 20 °C for 36 h (instead of 30 °C overnight) to maximize the amount of soluble protein. From 1 L of cell culture, ~30 mg of homogeneous protein was obtained, which was concentrated to 12 mg/mL in 10 mM NaH<sub>2</sub>PO<sub>4</sub> buffer (pH 7.5). DLS analysis indicated that the mutant enzyme formed a trimer in solution. Crystallization screening resulted in the growth of a single crystal (300  $\times$  150  $\times$  100  $\mu$ m<sup>3</sup>) that was obtained after 4 weeks in a sitting-drop vapor-diffusion experiment from condition B9 of the Morpheus screen (Molecular Dimensions). With this crystal, 1.55 Å resolution X-ray diffraction data were collected in-house at 110 K using a Microstar rotating-anode X-ray source (Bruker AXS GmbH) in combination with Helios optics (Incoatec GmbH) and a MAR345dtb detector (Marresearch GmbH). X-ray data were integrated using the program XDS and further processed with the program Aimless, as described for the data obtained with wild-type RhCC.<sup>22</sup> The crystal belonged to space group C2 and contained a protein trimer in the asymmetric unit (solvent content = 49%). The wild-type RhCC structure was used as a molecular replacement search model to obtain an initial structure. Subsequent model building and refinement of the D106A structure was carried out with the programs Coot, Refmac5, and phenix.refine.<sup>21</sup> A summary of the data collection and model refinement statistics is given in the Supporting Information (Table S).

**Crystal Structure Analysis.** MolProbity was used for validating the stereochemical quality of the models.<sup>23</sup> Structure-based sequence alignments were carried out using the protein-structure comparison service Fold at the European Bioinformatics Institute (PDBFold)<sup>24</sup> and visualized using Jalview.<sup>25</sup> Superpositions and calculation of C $\alpha$ -backbone RMSD values were carried out using PDBFold. The CheckMyMetal web server was used to validate the metal-binding site.<sup>26</sup> PyMOL (Schrödinger) was used for structure analysis and figure preparations. Coordinates for the structures of wild-type (1.78 Å) and mutant D106A (1.55 Å) RhCC have been deposited with the Protein Data Bank (4USP and 4USR, respectively).

**Enzyme Assays.** The conversion of 4HPP by RhCC was monitored in 10 mM Na<sub>2</sub>HPO<sub>4</sub> buffer (pH 7.3) at 22 °C. The reaction was initiated by the addition of 4HPP from a stock solution to yield a final concentration of 100–200  $\mu$ M in a cuvette containing 1 mL of 10 mM Na<sub>2</sub>HPO<sub>4</sub> buffer (pH 7.3) and 10–20  $\mu$ g of RhCC. Stock solutions of 4HPP were made by dissolving the appropriate amount of the free acid in absolute ethanol. The crystalline free acid of 4HPP is exclusively in the enol form. UV–vis spectra were recorded

between 200 and 400 nm with time intervals of 60 or 120 s. A decrease of the absorbance at 290 nm indicates depletion of 4HPP ( $\lambda_{\text{max}} = 290$  nm). The reaction that was carried out to examine the spontaneous nonenzymatic ketonization of 4HPP was executed as described above, except that no enzyme was added to the reaction buffer.

For kinetics assays, an appropriate amount of enzyme (from a 10 mg/mL stock solution) was diluted in 50 mL of 10 mM  $\text{Na}_2\text{HPO}_4$  buffer (pH 7.3) or 50 mL of 10 mM  $\text{Na}_2\text{HPO}_4$  buffer (pH 8.3), after which the mixture was allowed to equilibrate for 1 h at 22 °C. Substrate concentrations ranged between 0.025 and 2.75 mM. At each substrate concentration, the rate of spontaneous nonenzymatic ketonization was determined and subtracted from the observed rate of depletion of 4HPP in the presence of enzyme.

The RhCC-catalyzed conversion of 4HPP under anaerobic conditions, using glucose and glucose oxidase, was carried out as follows. A small scale reaction was carried out at 22 °C in a 25 mL glass reaction vial that was equipped with a septum and a magnetic stirrer bar, to which was added 10 mL of 10 mM  $\text{Na}_2\text{HPO}_4$  buffer (pH 7.3) supplemented with 100  $\mu\text{g}/\text{mL}$  RhCC. Molecular oxygen was purged from the reaction buffer by applying a constant flow of nitrogen gas through the reaction vial for 2 h. Subsequently, to ensure and to maintain reaction conditions devoid of molecular oxygen, glucose (1 M stock solution in 10 mM  $\text{Na}_2\text{HPO}_4$  buffer, pH 7.3) was added to a final concentration of 15 mM, and glucose oxidase was added to a final concentration of 25  $\mu\text{g}/\text{mL}$  (2 mg/mL stock solution in  $\text{H}_2\text{O}$ ). Next, 4HPP (100 mM stock solution in absolute ethanol) was added to the reaction mixture to a concentration of 100  $\mu\text{M}$ . A 1.5 mL sample was drawn from the reaction mixture directly after the addition of the substrate and transferred to a 1 cm quartz cuvette that was sealed airtight with a lid. The volume of the sample ensured that the cuvette was completely filled with sample, thereby minimizing the possibility of air bubbles remaining after the sealing of the cuvette. The reaction was monitored by UV-vis spectroscopy, and spectra were recorded every 2 min.

**HPLC Detection of Enzymatic Products.** Separation of the various products of the RhCC-catalyzed conversion of 4HPP was achieved by a reverse-phase HPLC method. HPLC was carried out on an analytical HPLC device that was equipped with a Shimadzu LC-10 AT pump and a Shimadzu SPD-M10A diode array detector. Separation of the compounds in the reaction mixture was achieved using an Agilent Eclipse XDB-C18 column (250  $\times$  4.6 mm, 5  $\mu\text{m}$ ) as the stationary phase and  $\text{H}_2\text{O}$  (eluent A) and absolute methanol (eluent B), both supplemented with 1% formic acid, as the mobile-phase ingredients. The gradient program was as follows: 0–7 min, 100% eluent A; 7–30 min, linear gradient to 30% eluent B; 30–31 min, linear gradient to 100% eluent B; 31–37 min, 100% eluent B; 37–38 min, linear gradient to 100% eluent A; 38–47 min, 100% eluent A. The flow rate and temperature were maintained at constant values: 800  $\mu\text{L}/\text{min}$  and 25 °C, respectively. The sample-injection volume ranged between 20 and 100  $\mu\text{L}$ , depending on the concentration of the products in the sample. The products were detected by the diode array detector at 230, 250, and 300 nm.

The HPLC chromatogram (Supporting Information Figure 6) and the data represented by the progress curves (Supporting Information Figure 7) were obtained by performing a batch conversion of 4HPP by RhCC and analyzing samples taken at specific time points by the HPLC method described above. The

batch conversion of 4HPP by RhCC was carried out at 22 °C in 12.0 mL of 10 mM  $\text{Na}_2\text{HPO}_4$  buffer (pH 7.3) that was supplemented with 40  $\mu\text{g}/\text{mL}$  RhCC. The reaction was initiated by the addition of 60  $\mu\text{L}$  of a stock solution of 4HPP (100 mM in absolute ethanol), yielding a final concentration of 500  $\mu\text{M}$ . Samples (500  $\mu\text{L}$  each) were withdrawn at the appropriate time intervals and directly mixed with 500  $\mu\text{L}$  of 100 mM  $\text{Na}_2\text{HPO}_4$  buffer (pH 6.0) in an Eppendorf tube. This ensured that the pH of the sample was reduced to pH 6.0, at which the activity of RhCC is completely quenched. Samples were flash-frozen in liquid  $\text{N}_2$  until further analysis, or directly applied to a Vivaspin centrifugal concentrator equipped with a 5000 Da molecular weight cutoff filtration membrane (Sartorius Stedim Biotech S.A., France) and centrifuged at 4000 rpm for 2 min in order to remove all protein from the sample. The flow-through was subsequently analyzed by HPLC.

**Batch Conversion of 4HPP by RhCC for Analysis by  $^1\text{H}$  NMR Spectroscopy.** Because of the inhibition of RhCC at substrate concentrations exceeding 1 mM at pH 7.3, multiple additions of substrate to a batch reaction were needed in order to achieve a concentration of products that was sufficient for detection by  $^1\text{H}$  NMR spectroscopy. A batch reaction was typically carried out at 22 °C in a 25 mL glass reaction vial with a septum and a magnetic stirrer bar, to which was added 8.25 mL of 10 mM  $\text{Na}_2\text{HPO}_4$  buffer (pH 9.2) that was supplemented with 100  $\mu\text{g}/\text{mL}$  wild-type RhCC and 750  $\mu\text{L}$   $\text{D}_2\text{O}$ . The reaction was initiated by the addition of 1 mL of 10 mM  $\text{Na}_2\text{HPO}_4$  buffer (pH 7.3) in which 3.6 mg of crystalline 4HPP was dissolved directly before the start of the reaction. The reaction mixture was placed under a constant flow of molecular oxygen through the septum and constant stirring, ensuring that no oxygen limitation could occur during the course of the reaction. Reaction progress was determined by the UV-vis spectroscopic analysis of 20  $\mu\text{L}$  samples taken from the reaction mixture. Typically, 3.6 mg of 4HPP was fully converted in a 30 min reaction time. Once the reaction was completed, 1 mL of the reaction mixture was extracted from the reaction vial and used to dissolve another amount of 3.6 mg of crystalline 4HPP, which was subsequently added back to the reaction system for conversion by RhCC. This process was repeated six times in order to achieve sufficiently high concentrations of each product. Upon completion of the reaction after the addition of the final amount of 4HPP (the final reaction mixture was pH 7.1), a 600  $\mu\text{L}$  sample was taken and analyzed by  $^1\text{H}$  NMR spectroscopy.

The RhCC-catalyzed conversions of 4HPP that were analyzed with HPLC and  $^1\text{H}$  NMR spectroscopy were conducted at different pH values: HPLC analysis was carried out at pH 7.3; for  $^1\text{H}$  NMR, the pH of the initial reaction mixture was set to 9.2 to allow for the decrease of pH that followed multiple additions of 4HPP substrate. However, an HPLC chromatogram recorded from the reaction mixture obtained at pH 9.2 showed high similarity with that recorded from the reaction mixture obtained at pH 7.3, demonstrating that identical products are formed at both pH values. The only exception is that the HPLC chromatogram as well as the  $^1\text{H}$  NMR spectrum indicated the absence of the keto form of 4HPP in the reaction mixture obtained at pH 9.2, whereas the HPLC chromatogram did indicate trace amounts of the keto form of 4HPP in the reaction mixture obtained at pH 7.3. Control experiments (at pH 7.3 and 9.2) demonstrated that

4HPP undergoes ketonization in the absence of enzyme without the detectable formation of oxygenation products.

**Structure Determination of Products 1 and 2 by CryoNMR Spectroscopy.** The structures of products 1 (3-hydroxy-3-(4-hydroxyphenyl)-pyruvate) and 2 (4-hydroxybenzaldehyde) were determined by CryoNMR spectroscopy (Spinovation Analytical B.V., Oss, The Netherlands). A 10 mg amount of 4HPP was converted into products at 22 °C in a reaction mixture consisting of 70 mL of 10 mM Na<sub>2</sub>HPO<sub>4</sub> buffer (pH 7.3) supplemented with 30 μg/mL RhCC. Reaction progress was monitored by UV–vis spectroscopic analysis. After the reaction had reached completion (30 min), RhCC was removed using a Vivaspin centrifugal concentrator equipped with a 5000 Da molecular weight cutoff filtration membrane. The protein-free flow-through was collected and subsequently freeze-dried overnight. The resulting lyophilizate was stored on ice prior to further analysis. CryoNMR spectra were recorded using a Bruker 500 MHz Avance III system (Bruker Biospin, Rheinstetten, Germany) that was equipped with a 5 mm cryo probe and a CPTCI probe (<sup>1</sup>H – <sup>13</sup>C/<sup>15</sup>N/<sup>2</sup>H + Z-gradients). Separation of the reaction products was achieved using the HPLC protocol described above and was carried out on an Agilent 1200 system (Agilent Technology, Santa Clara, CA, USA) that was equipped with an Agilent Eclipse XDB-C18 column (250 × 4.6 mm, 5 μm). Fractions containing products 1 and 2 were collected, freeze-dried, and dissolved in D<sub>2</sub>O prior to analysis. NMR spectra were recorded at 30 °C; depending on the complexity and concentration of each product, a set of NMR spectra (<sup>1</sup>H-1D, COSY, <sup>1</sup>H,<sup>13</sup>C-HSQC, <sup>1</sup>H,<sup>13</sup>C-HMBC) were recorded. Full spectroscopic data are given in the Supporting Information.

**Incubations with <sup>16</sup>O<sub>2</sub>, <sup>18</sup>O<sub>2</sub>, and H<sub>2</sub><sup>18</sup>O and High-Resolution LC-MS and MS/MS Analyses.** High-resolution LC-MS and MS/MS analyses were carried out on an LTQ-Orbitrap XL (Thermo Scientific, Bremen, Germany) coupled to a Shimadzu Prominence UFLC system (Shimadzu Corp., Kyoto, Japan) equipped with an Agilent Eclipse XDB-C18 column (250 × 4.6 mm, 5 μm), using the HPLC method described above.

Samples of a reaction carried out in aerated buffer were prepared as follows. A reaction was carried out at 22 °C in a quartz cuvette containing 1 mL of 10 mM Na<sub>2</sub>HPO<sub>4</sub> buffer (pH 7.3) supplemented with 50 μg RhCC. The reaction was initiated by the addition of 7.5 μL of a stock solution of 4HPP (100 mM in absolute ethanol), yielding a final 4HPP concentration of 500 μM, and the reaction was monitored in a UV–vis spectrophotometer. After a reaction time of ~5 min, at which time ~50% of the substrate 4HPP had been consumed, the enzyme was removed using a Vivaspin column (as described above), and a 100 μL sample of the flow through was directly injected into the HPLC system and analyzed by high-resolution LC-MS and MS/MS.

Samples of a reaction carried out in the presence of H<sub>2</sub><sup>18</sup>O were prepared as described above, with the following modification. The reaction buffer (1 mL) was prepared by mixing 500 μL of 20 mM Na<sub>2</sub>HPO<sub>4</sub> buffer (pH 7.3) with 500 μL of H<sub>2</sub><sup>18</sup>O.

Reactions in the presence of <sup>18</sup>O<sub>2</sub> (and in the absence of <sup>16</sup>O<sub>2</sub>) were carried out using a closed airtight reaction system (Supporting Information Figure 8, arrow 1) that was built of metal tubes, fittings, and valves (Swagelok Company, Solon, Ohio, USA) to which a reaction container (Supporting Information Figure 8, arrow 2), a vacuum pump, and a small

gas cylinder containing <sup>18</sup>O<sub>2</sub> (Supporting Information Figure 8, arrow 3) were attached. The reaction container consisted of two small flasks connected to one another by a glass tube. A single outlet (Supporting Information Figure 8, arrow 4) allowed this to be attached to the airtight reaction system so that the reaction buffer could be degassed and subsequently equilibrated in <sup>18</sup>O<sub>2</sub>. A reaction in the presence of <sup>18</sup>O<sub>2</sub> was carried out as follows. The reaction buffer (3 mL, 10 mM Na<sub>2</sub>HPO<sub>4</sub> buffer, pH 7.3) that was supplemented with RhCC (50 μg/mL) was added to one of the flasks of the reaction container, whereas 4HPP was added to the other reaction container flask in an amount by which it would reach a final concentration of 500 μM in the reaction mixture. The amount of 4HPP was added from a stock solution in absolute ethanol. The ethanol was evaporated prior to connection of the reaction container to the airtight reaction system. Magnetic stir bars were added to each flask to allow for adequate mixing. Once assembled, the reaction system was placed under vacuum (Supporting Information Figure 8, arrow 5) for 15 min in order to remove air from the system and to purge the reaction buffer containing RhCC of dissolved gases, including <sup>16</sup>O<sub>2</sub>. Subsequently, a valve that connected the vacuum pump to the reaction system was closed, and <sup>18</sup>O<sub>2</sub> was allowed to fill the reaction system until it had reached atmospheric pressure (Supporting Information Figure 8, arrow 3). The reaction buffer containing RhCC was equilibrated with <sup>18</sup>O<sub>2</sub> for 30 min prior to reaction initiation. The reaction was started by inverting the reaction container so that the reaction buffer containing RhCC could flow into the second reaction flask containing the now-solid 4HPP, allowing 4HPP to dissolve in the reaction buffer. After 10–15 min of reaction time, the reaction container was disconnected from the reaction system, and a sample of the reaction mixture was prepared for LC-MS and MS/MS analysis as described above.

Product 3 (oxalic acid) could be detected by high-resolution LC-MS using the HPLC method described above. Because of the high polarity of 3, it ended up in the void volume of the reverse-phase C18 column, but it was thus separated from the other reaction products. To further establish the identity of 3 as oxalic acid, a second HPLC method was developed using an Waters XBridge amide column (4.6 × 150 mm<sup>2</sup>, 3.5 μm; Waters Corporation, Milford, MA, USA). An isocratic flow of 20 mM NH<sub>4</sub>HCO<sub>3</sub> buffer (pH 7.0) containing 50% (v/v) acetonitrile using a flow rate of 0.5 mL/min allowed the oxalic acid to be retained on the column for an appropriate retention time. The composition of the eluent allowed for the detection of oxalic acid on the LTQ Orbitrap XL system.

## RESULTS

**Purification of RhCC.** By sequence similarity, the hypothetical protein YP\_702633.1 (referred to herein as RhCC) of *R. jostii* RHA1 most resembles the members of the *cis*-3-chloroacrylic acid dehalogenase (*cis*-CaaD) family within the tautomerase superfamily.<sup>27–29</sup> Despite this relationship to enzymes with known activity, the substrate preference of RhCC is anything but clear. To determine its structure and function, RhCC was produced as a C-terminal His<sub>6</sub>-tagged protein in *E. coli* BL21(DE3) and purified to near homogeneity using Ni-based immobilized-metal affinity chromatography (Supporting Information Figure 1). Analysis of RhCC by electrospray ionization-mass spectrometry (ESI-MS) showed one major protein species with a mass of 18 489 ± 1 Da. A comparison of this value to the calculated subunit mass (18 620

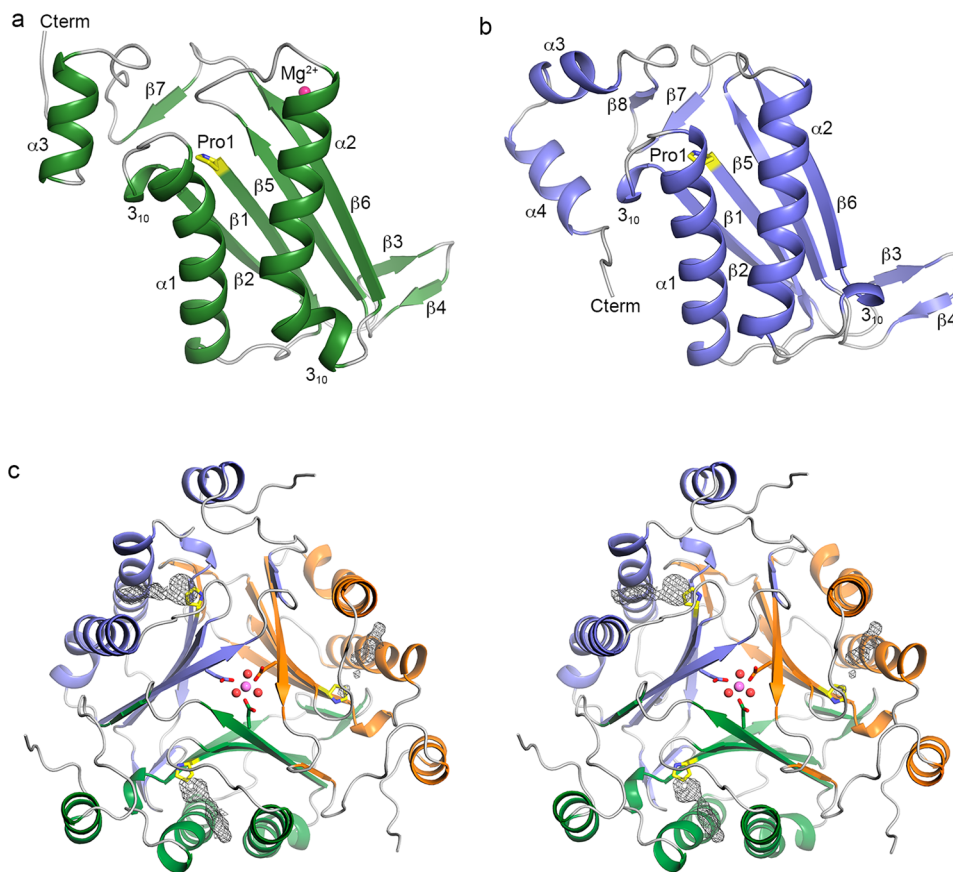


**Figure 1.** Overall structure of RhCC and its comparison with *cis*-CaaD. (a) Ribbon representation (green) of a single RhCC subunit. Pro1 is drawn as sticks (yellow), and the  $Mg^{2+}$  ion is violet. Secondary structure elements are labeled. (b) Ribbon representation (blue) of a single *cis*-CaaD subunit (PDB entry 2FLZ). (c) Stereo view of the RhCC trimer in ribbon representation, with the three subunits drawn in different colors. The Pro1 residues are drawn as sticks (yellow), whereas the  $Mg^{2+}$  ion (violet sphere) at the center of the trimer is shown together with its coordinating ligands: three Asp106 residues (sticks, different colors) and three water molecules (red spheres). Also shown is the difference electron density ( $F_o - F_c$ ) of the unidentified ligand bound at the three putative active sites.

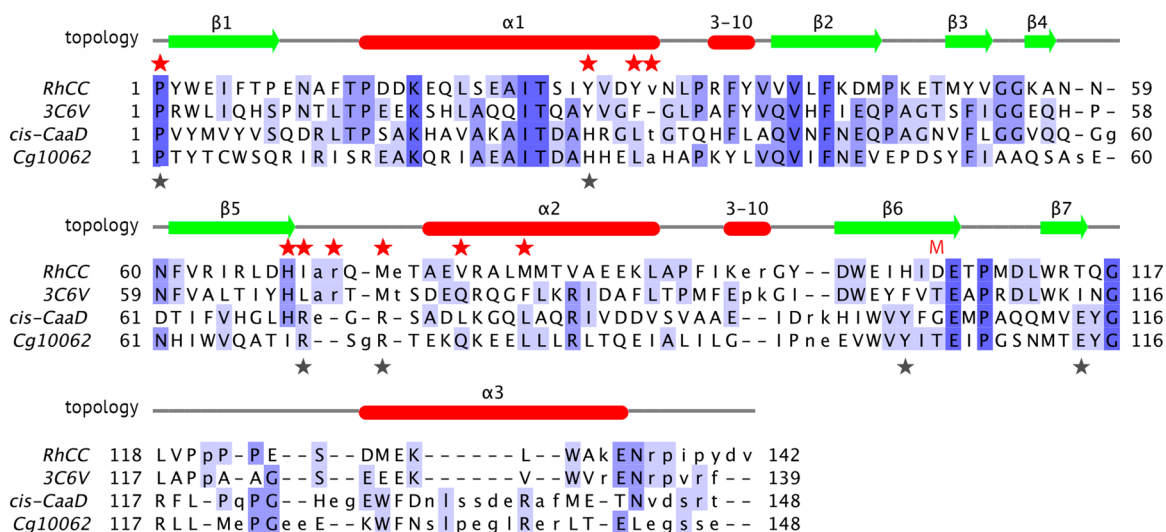


**Figure 2.** Structure-based multiple sequence alignment of RhCC, 3C6V, *cis*-CaaD and Cg10062. This alignment was produced using the programs T-coffee<sup>24</sup> and JalView.<sup>25</sup> Residues belonging to the common structural core of the proteins are shown in capital letters. The secondary structure topology is derived from the RhCC structure. Red and black asterisks mark residues surrounding the unidentified bound ligand at the putative active site of RhCC, and the active site residues of *cis*-CaaD, respectively (see also Figure 3). The metal-coordinating residue of RhCC (Asp106) is labeled with a red M.

Da) indicates that the translation-initiating methionine is removed during posttranslational processing, which results in

a mature protein that is 145 amino acids long with an N-terminal proline. The native molecular mass of RhCC was

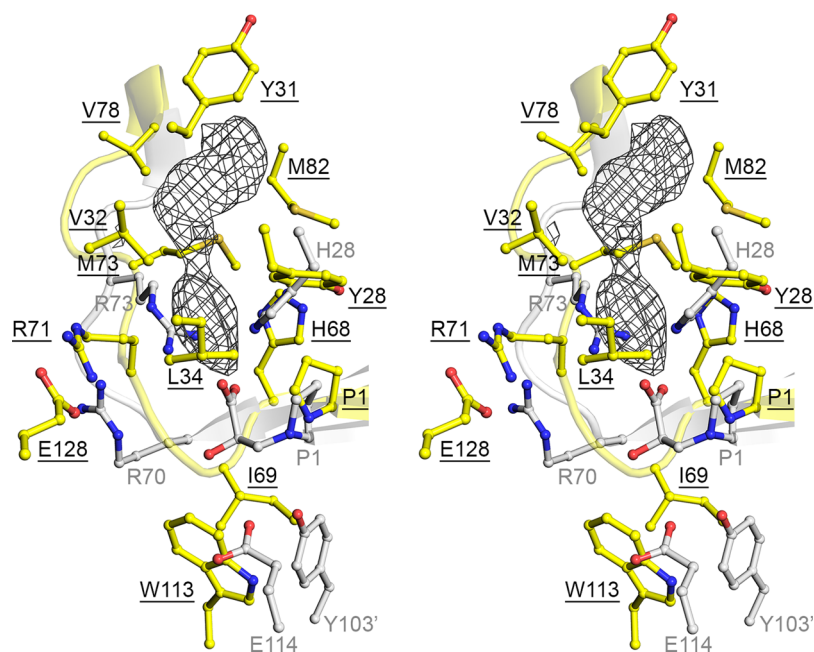


**Figure 3.** Stereo view of the putative-active-site region of RhCC and its comparison with the active site of inactivated *cis*-CaaD. The putative-active-site region of RhCC is shown as ball-and-sticks with yellow carbons, whereas the active site of inactivated *cis*-CaaD (PDB entry 2FLT) is shown as ball-and-sticks with white carbons. The covalently bound (*R*)-2-hydroxypropanoate adduct on Pro1 of *cis*-CaaD, which results from the inactivation of the enzyme by oxirane-2-carboxylate, is shown. Also shown, as a gray mesh, is the difference electron density ( $F_0 - F_c$ ) for the unidentified bound ligand in RhCC (1.78 Å resolution, contoured at 2.5  $\sigma$ ). Oxygen and nitrogen atoms are colored red and blue, respectively. Residues of RhCC are indicated with black underlined labels, whereas residues of *cis*-CaaD are indicated with gray labels. The apostrophe on Y103' signifies that this residue belongs to a neighboring subunit.

estimated by DLS to be ~53 kDa, which suggests that the native protein exists as a homotrimer in solution.

**Overall Structure of Native RhCC.** To enhance our understanding of the relationship between RhCC and members of the *cis*-CaaD family within the tautomerase superfamily, we have determined the crystal structure of native RhCC. The RhCC structure was solved at 1.78 Å resolution by molecular-replacement methods and refined to *R* and *R*<sub>free</sub> values of 15.2 and 18.7%, respectively. The asymmetric unit in the crystal contains one homotrimer and has a solvent content of 47%. The overall fold of the individual subunits of the trimer and their mode of association are very similar to those observed in the structures of *cis*-CaaD and Cg10062 (a *cis*-CaaD homologue from *Corynebacterium glutamicum*, PDB entry 3N4D), despite the low sequence identity between RhCC and these two proteins (14–16%; Figures 1 and 2 and Supporting Information Figure 2).<sup>30,31</sup> Residues 1–123 form the core of the individual RhCC subunits, containing the two  $\beta$ - $\alpha$ - $\beta$  structural motifs that are characteristic of the tautomerase superfamily fold.<sup>13</sup> Strands  $\beta$ 1,  $\beta$ 2,  $\beta$ 5, and  $\beta$ 6 of the two  $\beta$ - $\alpha$ - $\beta$  structural motifs associate into a four-stranded  $\beta$  sheet within each RhCC subunit. The three additional  $\beta$  strands ( $\beta$ 3,  $\beta$ 4, and  $\beta$ 7) are important for subunit–subunit interactions because they complement the central  $\beta$  sheets of the neighboring subunits in the RhCC trimer. Residues 124–142 form a short  $\alpha$ -helical extension at the C terminus of each RhCC subunit, which is also present in the *cis*-CaaD and Cg10062 structures but with more structural divergence as compared to the N-terminal cores of these proteins. *C* $\alpha$ -backbone superpositions of the RhCC trimer with its structural homologues resulted in a root-mean-square deviation (RMSD) of 2.5 Å with *cis*-CaaD (PDB entry 2FLZ, 334 equiv *C* $\alpha$  atoms) and 2.4 Å with Cg10062 (PDB entry 3N4D, 334 equiv *C* $\alpha$

atoms). Significantly higher structural similarity was observed between RhCC and the structure of a putative tautomerase from the thermophilic fungus *A. fumigatus* (PDB code 3C6V), resulting in a sequence identity between the two proteins of 40% (Figure 2) and an RMSD in the *C* $\alpha$ -backbone conformation of 1.4 Å (398 equiv *C* $\alpha$  atoms within the trimers). The implications of this structural similarity for the function of RhCC are unknown because of the lack of functional data for the *A. fumigatus* protein.

**Metal-Binding Site.** Unlike the structures of *cis*-CaaD, Cg10062 and the *A. fumigatus* protein, the RhCC crystal structure reveals the presence of a metal-binding site on the surface of the trimer. The metal-binding site is positioned at the noncrystallographic 3-fold symmetry axis, near the C-terminal ends of the three trimer-related  $\beta$ 6 strands, with residue Asp106 from each subunit acting as metal-coordinating ligand (Supporting Information Figure 3a). Three carboxylate oxygen atoms of the trimer-related aspartate residues and three water molecules coordinate the metal ion in an octahedral geometry. The high-resolution X-ray data allowed an accurate determination of the oxygen–metal bond distances (2.1–2.2 Å); together with the observed coordination geometry, this is consistent with the presence of either Mg<sup>2+</sup>, Zn<sup>2+</sup>, or Mn<sup>2+</sup>. Additional analyses of *B* factors and anomalous electron-density maps, complemented by validation with the CheckMyMetal web server, strongly suggest that the bound metal ion is Mg<sup>2+</sup>.<sup>26</sup> The distance between the metal ion and the N-terminal proline residues is 15 Å.

**Putative Active Site.** Based on the structural similarities with *cis*-CaaD and Cg10062, we expect the RhCC trimer to contain three active sites that are defined by the locations of the N-terminal proline residues (Figure 1 and Supporting Information Figure 2). The observation of extra electron



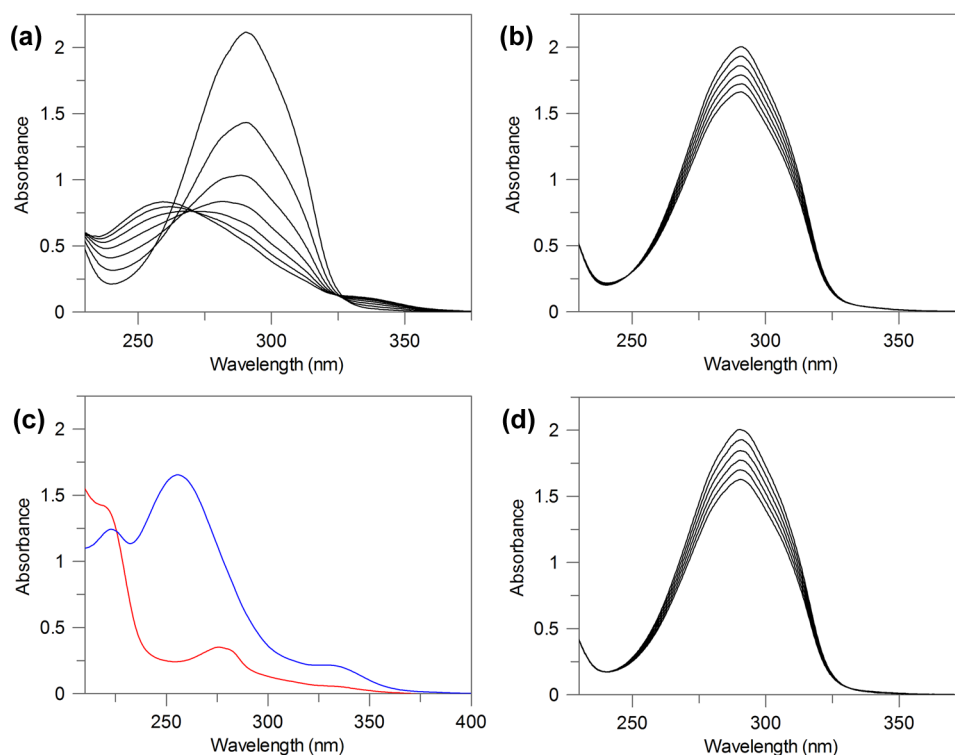


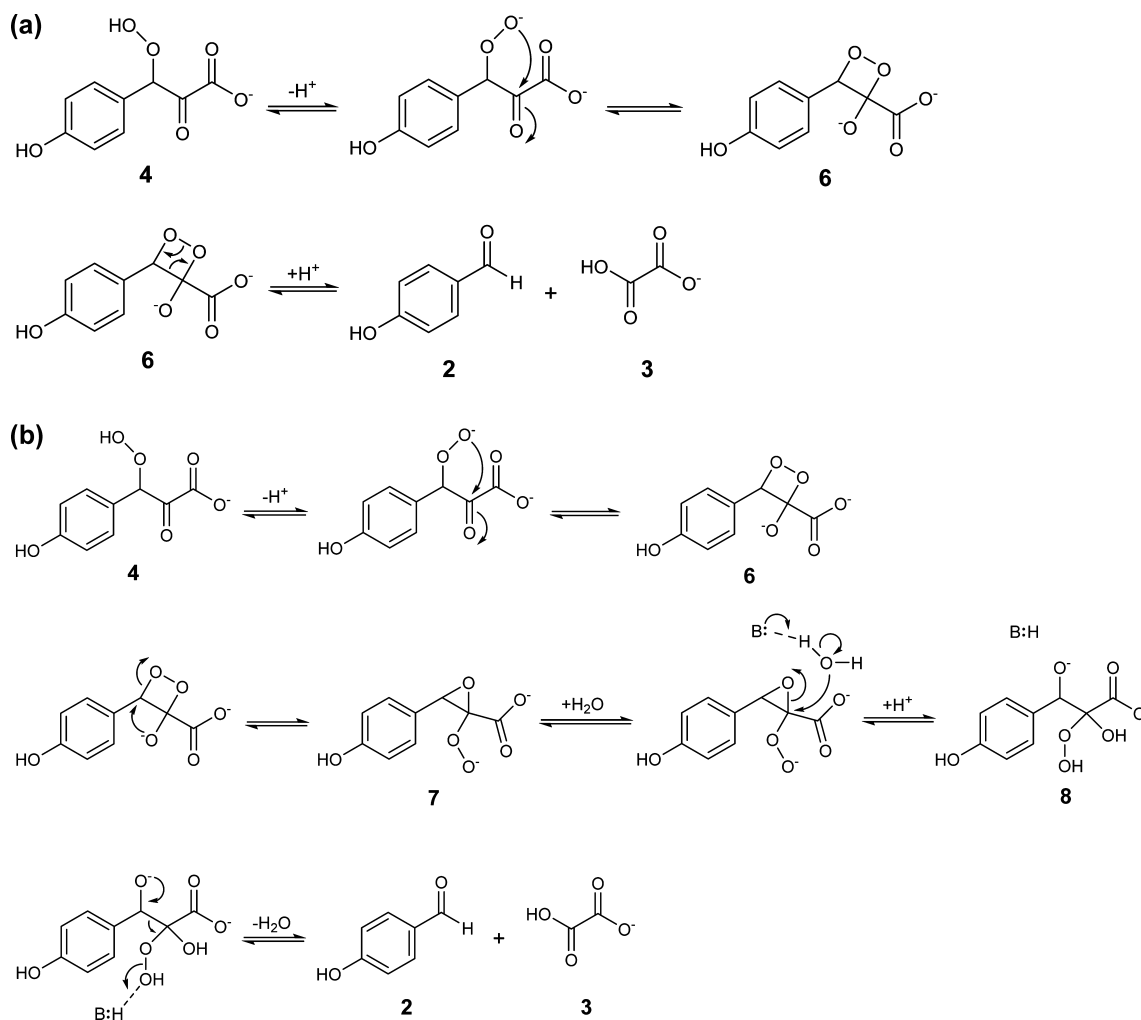
**Figure 4.** UV-vis spectroscopic analysis of the unusual enzymatic activity of RhCC. (a) UV-vis spectra monitoring the RhCC-catalyzed conversion of 4HPP (100  $\mu\text{M}$ ) in aerated 10 mM  $\text{Na}_2\text{HPO}_4$  buffer (pH 7.3). Spectra were recorded every 2 min. These spectra clearly indicate that the enol form of 4HPP ( $\lambda_{\text{max}} = 290$  nm) is rapidly consumed during the course of the reaction, resulting in a product mixture with a characteristic UV-vis spectrum ( $\lambda_{\text{max}} = 257$  nm). (b) UV-vis spectra monitoring the spontaneous nonenzymatic ketonization of 4HPP (100  $\mu\text{M}$ ) in aerated 10 mM  $\text{Na}_2\text{HPO}_4$  buffer (pH 7.3). Spectra were recorded every 2 min. (c) A comparison of the UV-vis spectrum of the keto form of 4HPP (red) and that of the reaction mixture after completion of the reaction of RhCC with 4HPP (blue). The keto form of 4HPP was obtained by spontaneous nonenzymatic ketonization of 4HPP (200  $\mu\text{M}$ ) in 10 mM  $\text{Na}_2\text{HPO}_4$  buffer (pH 7.3, 120 min reaction time). The reaction mixture of the RhCC-catalyzed conversion of 4HPP was obtained by the addition of 4HPP (200  $\mu\text{M}$ ) to 10 mM  $\text{Na}_2\text{HPO}_4$  buffer (pH 7.3) supplemented with RhCC (2  $\mu\text{M}$ ). The spectrum was recorded after 10 min reaction time. (d) UV-vis spectra monitoring the RhCC-catalyzed conversion of 4HPP (100  $\mu\text{M}$ ) under anaerobic conditions in 10 mM  $\text{Na}_2\text{HPO}_4$  buffer (pH 7.3) in the presence of 15 mM glucose and 25  $\mu\text{g}/\text{mL}$  glucose oxidase. Spectra were recorded every 2 min.

densities near the three N-terminal proline residues indicates the presence of a bound ligand (Figures 1c and 3). Unfortunately, the features of the electron densities are insufficiently detailed to allow identification of the bound ligand. Residues surrounding the unidentified ligand in each RhCC subunit are Pro1; Tyr28, Tyr31, Val32, and Leu34 ( $\alpha 2$  helix); His68 ( $\beta 5$  strand); Arg71 and Met73 ( $\beta 5$ - $\alpha 2$  loop); and Val78 and Met82 ( $\alpha 2$  helix). Although the location of this putative active site in a RhCC subunit coincides well with that observed in the *cis*-CaaD and Cg10062 subunits, the surrounding residues are very different. In *cis*-CaaD and Cg10062, five conserved active-site residues, in addition to the N-terminal proline, were shown to be critical for the hydrolytic dehalogenation reaction catalyzed by these enzymes (in *cis*-CaaD these residues are His28, Arg70, Arg73, Tyr103', and Glu114, with the apostrophe signifying that the residue comes from a neighboring subunit). None of these five residues are conserved in RhCC (Figure 2). In addition, the conformation of the  $\beta 5$ - $\alpha 2$  loop, which is a critical component of the active sites in *cis*-CaaD and Cg10062, is significantly different in RhCC because of the insertion of two extra residues. In *cis*-CaaD and Cg10062, the  $\beta 5$ - $\alpha 2$  loop contains two catalytically important arginine residues: Arg70 and Arg73. In RhCC, the single arginine residue present in the  $\beta 5$ - $\alpha 2$  loop, Arg71, takes up a position that is somewhat in between those of Arg70 and Arg73 in the *cis*-CaaD structure. However,

the side chain of Arg71 in RhCC points away from the putative active site and toward the C-terminal helix, to which it is stabilized by a salt-bridge interaction with Glu128 (Figure 3). Overall, the putative active site in RhCC seems more hydrophobic than the active sites in *cis*-CaaD and Cg10062. Also, the direct environment of the N-terminal proline in RhCC is more hydrophobic than in *cis*-CaaD and Cg10062, with Ile69 and Trp113 in RhCC occupying similar 3D positions as Tyr103' and Glu114 in *cis*-CaaD and Cg10062. The prolyl nitrogen atom of Pro1 in RhCC forms two hydrogen bond interactions with surrounding residues: one direct hydrogen bond with the main-chain carbonyl oxygen of Tyr38 and a water-bridged hydrogen bond with the main-chain amide nitrogen atom of Ile69.

**Unusual Enzyme Activity.** Having established that RhCC belongs to the tautomerase superfamily, the enzyme was assayed for activity toward several available substrates of previously characterized members of this superfamily. Unlike its structural homologues *cis*-CaaD and Cg10062, RhCC does not catalyze the hydrolytic dehalogenation of *cis*-3-chloroacrylic acid (or the corresponding *trans* isomer), which is consistent with the lack of conservation of key catalytic residues of *cis*-CaaD and Cg10062 in RhCC (Figures 2 and 3). However, during the course of activity screening, RhCC was found to accept 4HPP as a substrate; 4HPP is a known substrate of the well-characterized tautomerase superfamily member macro-

Scheme 1. Oxidative Substrate Cleavage Catalyzed by RhCC



<sup>a</sup>A possible mechanism for the decomposition of hydroperoxide 4, as proposed by Jefford et al.<sup>33</sup> <sup>b</sup>A proposed mechanism for the formation of 2 and 3 that is based on hydroperoxide 4 functioning as the presumed initial enzymatic oxygenation product formed.

phage migration inhibitory factor (MIF, also known as phenylpyruvate tautomerase). MIF catalyzes the enol–keto tautomerization of 4HPP, utilizing its amino-terminal proline (Pro1) as the catalytic base (Supporting Information Scheme 1).<sup>32</sup>

To probe the nature of the reaction catalyzed by RhCC, the enzyme was incubated with 4HPP and the conversion was monitored by UV–vis spectroscopy (Figure 4). The spectra indicate that 4HPP ( $\lambda_{\max} = 290$  nm) is rapidly consumed by RhCC during the course of the reaction (Figure 4a,b). However, to our surprise, the RhCC-catalyzed conversion of 4HPP did not result in formation of the keto form of 4HPP but rather in the formation of a mixture of products with a characteristic UV–vis spectrum that is clearly different from that of the keto form of 4HPP (Figure 4c). Control experiments indicated that the keto form of 4HPP, which was prepared by spontaneous nonenzymatic ketonization of 4HPP, is not accepted as a substrate by RhCC; hence, although RhCC has the catalytic capacity to convert 4HPP, it does not function as an enol–keto tautomerase.

By monitoring the depletion of 4HPP by UV–vis spectroscopy, we were able to gain insight into the kinetics of the reaction catalyzed by RhCC. The enzyme was found to be

inactive below pH 6.0; at higher pH values, the activity of the enzyme increases. The catalytic efficiency (in terms of apparent  $k_{\text{cat}}/K_m$ ) was estimated to be  $2.5 \times 10^3$  and  $4.7 \times 10^4$   $M^{-1} s^{-1}$  at pH 7.3 and 8.3, respectively. The enzyme showed inhibition at increasing substrate concentrations, but the exact type of inhibition could not be established. Hence, the individual values of  $k_{\text{cat}}$  and  $K_m$  could not be determined. The highest observed reaction rates were 1.4 and 6.6  $s^{-1}$  at pH 7.3 and 8.3, respectively (Supporting Information Figure 4a,b).

**Identification of the Products of the RhCC-Catalyzed Conversion of 4HPP.** To identify the products of the RhCC-catalyzed conversion of 4HPP, we carried out the reaction at semipreparative scale and under constant flow of molecular oxygen. After the reaction was completed (as indicated by UV–vis spectroscopic analysis), a sample was taken from the reaction mixture and analyzed by  $^1H$  NMR spectroscopy. The spectrum indicated the formation of a rather complex mixture of products (Supporting Information Figure 5). As its characteristic signals at 7.68, 6.94, and 6.36 ppm (in  $D_2O$ ) could not be observed, it was inferred that 4HPP was completely consumed. The keto form of 4HPP was present in the reaction mixture (7.16, 6.91, and 4.03 ppm). However, its presence is not caused by the action of RhCC but by the

nonenzymatic ketonization of 4HPP as verified by control experiments (Figure 4b,d).

To identify the products that give rise to the major peaks observed in the  $^1\text{H}$  NMR spectrum, a reverse-phase HPLC experiment was set up to separate and isolate the various reaction products for full characterization by NMR and mass spectroscopy (Supporting Information Figure 6). The eluents in the HPLC experiment were chosen so that they are compatible with high-resolution LC-MS and MS/MS analysis. This enabled us to determine the exact mass and elemental composition of the major products and product ion scans at high resolution provided additional insight into the molecular structures. The exact mass data related to the most prominent peaks in the HPLC chromatogram and the NMR data of lyophilized fractions that correspond to those peaks allowed us to identify 3-hydroxy-3-(4-hydroxyphenyl)-pyruvate (**1**, Supporting Information Figure 5) and 4-hydroxybenzaldehyde (**2**) as two major products of the RhCC-catalyzed conversion of 4HPP (Supporting Information). Products **1** and **2** eluted at 4.3 and 31.5 min, respectively, and  $^1\text{H}$  NMR data obtained from these fractions after lyophilization exactly match with the most intense signals in the  $^1\text{H}$  NMR spectrum that was recorded from the crude reaction mixture (Supporting Information Figure 5).

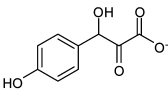
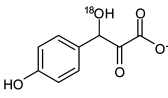
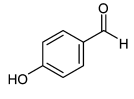
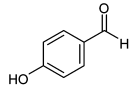
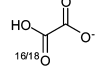
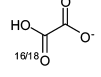
The products responsible for peaks A and B in the HPLC chromatogram of the crude reaction mixture could not be identified (Supporting Information Figure 6). The lyophilized fraction corresponding to peak A did not provide coherent spectroscopic data, indicating that the product responsible for peak A is unstable. The  $^1\text{H}$  NMR spectrum of the lyophilized fraction corresponding to peak B showed signals at  $\sim 6.6$ ,  $\sim 6.8$ , and  $6.95$  ppm, which match with minor absorptions in the  $^1\text{H}$  NMR spectrum of the crude reaction mixture (Supporting Information Figure 5). High-resolution LC-MS and MS/MS data related to peaks A and B (Supporting Information Table 1a,b) did not allow us to unambiguously identify the products corresponding to these peaks. We decided not to further pursue identification of the products responsible for peaks A and B because progress curves that were generated for all of the major products visible in the HPLC chromatogram (Supporting Information Figure 7b–e) show an initial lag phase with regard to the formation of the products corresponding to peaks A and B, indicating that they are not initial reaction products. In contrast, the progress curves of products **1** and **2** do not show an initial lag phase, which suggests that both **1** and **2** are initially formed products of the reaction or that both originate from a relatively quickly formed unstable intermediate that undergoes rapid decay. Accordingly, the progress curve of substrate 4HPP shows an initial linear decrease over time (Supporting Information Figure 7a).

Importantly, the identity of **2** implied the presence of yet another product based on a two-carbon unit, originating from the C1 and C2 atoms of 4HPP, that are evidently missing in product **2**. Indeed, high-resolution LC-MS data revealed the presence of oxalic acid (**3**, Scheme 1) in the reaction mixture, which could be confirmed by carrying out analytical high-resolution LC-MS with two different LC protocols and using oxalic acid as an authentic standard (Supporting Information Table 1c). The ability to detect **3** by high-resolution LC-MS allowed us to generate a progress curve for this product (Supporting Information Figure 7f); consistent with that observed for product **2**, the progress curve for **3** shows no initial lag phase.

The identification of **1**, **2**, and **3** as the major products of the RhCC-catalyzed conversion of 4HPP indicates that this enzyme catalyzes the incorporation of at least one atom of oxygen into substrate 4HPP; the C=C double bond of 4HPP is fully cleaved during the formation of **2** and **3**. This immediately raises questions about the source of the oxygen introduced into the substrate and the type of reaction that is catalyzed by RhCC.

**RhCC Is an Oxygenase.** As the conversion of 4HPP by RhCC is carried out in aerated buffer, either water or molecular oxygen ( $\text{O}_2$ ) is the source of the oxygen incorporated into products **1**–**3**. To elucidate the origin of the incorporated oxygen, reactions of RhCC with 4HPP were carried out in the presence of  $\text{H}_2^{18}\text{O}$  or  $^{18}\text{O}_2$ , using an experimental setup that was built in-house (Supporting Information Figure 8); the resulting product mixtures were analyzed by high-resolution LC-MS and MS/MS. High-resolution MS spectral analysis showed that the incorporated oxygen atom in product **1** originates exclusively from molecular oxygen (Table 1).

**Table 1.**  $^{18}\text{O}$  Incorporation in Products 1–3 As Determined by High-Resolution LC-MS and MS/MS Analysis of Reaction Mixtures Obtained from RhCC-Catalyzed Conversion of 4HPP in Aerated Buffer Supplemented with  $\text{H}_2^{18}\text{O}$  or Buffer Equilibrated with  $^{18}\text{O}_2$

Product	$\text{H}_2^{18}\text{O}^a$	$^{18}\text{O}_2^b$
3-hydroxy-3-(4-hydroxyphenyl)-pyruvate ( <b>1</b> )		
4-hydroxybenzaldehyde ( <b>2</b> )		
Oxalic acid <sup>c</sup> ( <b>3</b> )		

<sup>a</sup>The reaction was carried out in 10 mM  $\text{Na}_2\text{HPO}_4$  buffer (pH 7.3) that contained 50% (v/v)  $\text{H}_2^{18}\text{O}$ . <sup>b</sup>The reaction was carried out in 10 mM  $\text{Na}_2\text{HPO}_4$  buffer (pH 7.3) that was degassed and subsequently placed under  $^{18}\text{O}_2$  at atmospheric pressure in a closed reaction system; this allowed the buffer to equilibrate with  $^{18}\text{O}_2$  prior to initiation of the reaction and to be kept under an  $^{18}\text{O}_2$  atmosphere during the course of the reaction. <sup>c</sup>Control experiments (Supporting Information) have shown that under the stated reaction conditions no  $^{18}\text{O}$  is incorporated into oxalic acid by spontaneous exchange of its carboxylate oxygens with  $\text{H}_2^{18}\text{O}$ .

Additionally, product ion spectra allowed us to identify the C3 carbon atom of **1** as the site of oxygenation (Supporting Information Table 2), thus providing insight into the nature of the reaction catalyzed by RhCC. Interestingly, product **3** shows oxygen incorporation both from water and molecular oxygen, whereas product **2** shows no  $^{18}\text{O}$ -isotope labeling under any of the tested conditions (Table 1 and Supporting Information Table 3). It was anticipated that product **2** would exchange its aldehyde oxygen rapidly with solvent-derived oxygen under the conditions of LC-MS analysis (pH 1.8). This was validated by incubating compound **2** in  $\text{H}_2^{18}\text{O}$  at pH 1.8. The anticipated almost-complete exchange of solvent-derived oxygen for its aldehyde oxygen was detected by high-resolution MS for

compound **2** when it was incubated for 3 min in H<sub>2</sub><sup>18</sup>O at pH 1.8 (Supporting Information).

To further establish that RhCC catalyzes an O<sub>2</sub>-dependent reaction with 4HPP, the reaction was carried out under anaerobic conditions. Reactions were carried out in airtight cuvettes, and oxygen was removed from the buffer by flushing with nitrogen gas and by the subsequent addition of glucose and glucose oxidase prior to reaction initiation. Reaction progress was monitored by UV–vis spectroscopy (Figure 4d). The results clearly show that the unusual catalytic activity of RhCC is dependent on molecular oxygen, as neither product formation ( $\lambda_{\text{max}} = 257 \text{ nm}$ ) or rapid loss of substrate is detected under anaerobic conditions. Notably, in the absence of molecular oxygen (as in its presence), RhCC does not catalyze the ketonization of 4HPP because the rate of consumption of 4HPP is the same as that observed for the nonenzymatic ketonization of 4HPP (Figure 4b,d). Separate control experiments have shown that glucose or glucose oxidase do not affect the substrate itself or the activity of RhCC.

**Mutagenesis of the Metal-Binding Site.** To investigate the importance of the bound Mg<sup>2+</sup> ion for the oxygenase activity of RhCC, a single site-directed mutant was constructed in which the metal-coordinating residue Asp106 (Supporting Information Figure 3a) was replaced by an alanine (mutant D106A). This mutation is expected to remove the metal-binding site, leading to the loss of the Mg<sup>2+</sup> ion. It was found that the oxygenase activity of the purified D106A mutant (apparent  $k_{\text{cat}}/K_{\text{m}} = 2.4 \times 10^3 \text{ M}^{-1} \text{ s}^{-1}$  at pH 7.3) was similar to that of wild-type RhCC, indicating that the mutation had no significant effect on catalytic efficiency. Analysis of purified D106A mutant protein by DLS revealed that the mutant protein, similar to wild-type RhCC, exists as a homotrimer in solution. The structural consequences of the D106A mutation were examined by determining the crystal structure of the mutant enzyme to a resolution of 1.55 Å. The crystallographic R factor for the final model is 16% ( $R_{\text{free}} = 17.4\%$ ). A comparison of the D106A structure with that of wild-type RhCC reveals only local and minor effects resulting from the mutation, leaving the overall architecture otherwise unchanged (Supporting Information Figure 3c). The  $\alpha$ -carbon backbones of the wild-type and D106A mutant enzyme superimpose with an RMSD of 0.34 Å. An additional short  $\alpha$  helix of about 10 residues is visible at the C termini of the D106A trimer, which is likely a result of better-defined electron density. The only other difference between the two structures is the loss of the metal-binding site on the surface of the D106A trimer (Supporting Information Figure 3a,b). As the D106A mutant exhibits full oxygenase activity but has no metal ion bound, we conclude that the oxygenase activity of RhCC is metal-independent.

## DISCUSSION

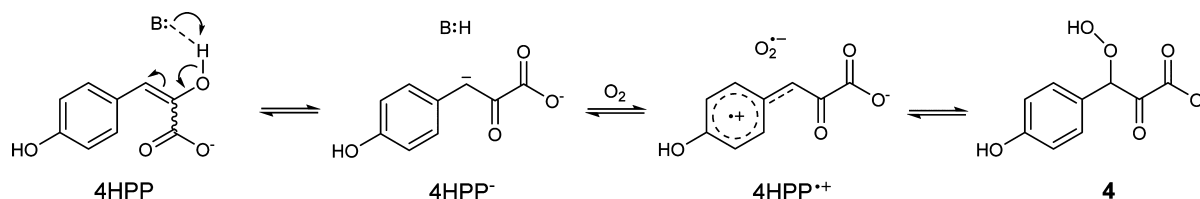
The radical-initiated nonenzymatic autoxidation of 4HPP has been studied in detail by Jefford et al.; this has led to the identification of several reaction products, including **2** and **3**.<sup>33</sup> The authors proposed that these are formed by the decomposition of 3-hydroperoxy-3-(4-hydroxyphenyl)-pyruvate (**4**, Scheme 1a) as the initial product of 4HPP autoxidation; the inherent instability of **4** prohibited its isolation. These findings suggest that the formation of **2** and **3** during the RhCC-catalyzed conversion of 4HPP could also be the result of a decomposition reaction of initially formed hydroperoxide **4**. However, the mechanism proposed by Jefford

et al.<sup>33</sup> for the formation of **2** and **3** (Scheme 1a) is inconsistent with the results obtained from our <sup>18</sup>O-labeling experiments carried out with RhCC because this mechanism would result in <sup>18</sup>O-labeled **2** in the presence of <sup>18</sup>O<sub>2</sub> and would not result in <sup>18</sup>O-labeled **3** in the presence of H<sub>2</sub><sup>18</sup>O, which is the opposite of our findings with RhCC. Although control experiments validated that any <sup>18</sup>O transferred to the aldehyde oxygen of **2** would be washed out under the conditions of LC-MS analysis, the enzymatic formation of <sup>18</sup>O-labeled **3** in incubations with substrate in H<sub>2</sub><sup>18</sup>O (exchange-in of solvent-derived oxygen for product **3** does not occur under the conditions used) suggests that products **2** and **3** may be formed in the RhCC-catalyzed conversion of 4HPP by a different mechanism than those proposed for the nonenzymatic autoxidation of 4HPP.

We therefore suggest an alternative mechanism, starting with presumed intermediate **4** or its deprotonated peroxyanionic analog, that could explain the formation of enzymatic products **2** and **3** (Scheme 1b). First, intramolecular attack of the peroxyanion on the carbonyl functional group of **4** leads to the formation of 4-(4-hydroxyphenyl)-3-oxido-1,2-dioxetane-3-carboxylate (**6**). Second, the oxyanion of dioxetane **6** may attack the C1 carbon of the dioxetane ring, resulting in the formation of 2-dioxidanide-3-(4-hydroxyphenyl)oxirane-2-carboxylate (**7**), by which the peroxide function of **4** has migrated from the C3 to the C2 position. Subsequently, hydrolysis of the epoxide and protonation of dioxidanide **7** results in the formation of 2-hydroperoxy-2-hydroxy-3-(4-hydroxyphenyl)-3-oxido-propanoate (**8**). Finally, the shift of one of the electron pairs of the 3-oxido functional group of **8** results in carbon–carbon bond cleavage and the concomitant expulsion of a hydroxyl ion (or water) from the 2-hydroperoxy group, leading to the formation of **2** and **3**. This proposed mechanism for the formation of **2** and **3** is consistent with the results obtained from our <sup>18</sup>O-labeling experiments carried out with RhCC.

We propose that product **1** may be formed as a result of the reaction between **4** and 4HPP (Supporting Information Scheme 2). There is precedent in the literature for reactions between organic hydroperoxides and alkenes that result in the formation of epoxides and alcohols.<sup>34</sup> Accordingly, **4** may react with 4HPP to result in the formation of **1** and 2-hydroxy-3-(4-hydroxyphenyl)oxirane-2-carboxylate (**5**). Because of the hydroxyl substituent on the epoxide ring, **5** is likely to rapidly isomerize, resulting in the formation of a second molecule of **1**. This mechanism is in agreement with the observation that the formation of **1** does not involve water and that the presence of <sup>18</sup>O<sub>2</sub> exclusively results in an <sup>18</sup>O-labeled C3 hydroxyl group.

Enzymes that catalyze reactions between organic substrates and molecular oxygen generally are dependent on cofactors such as flavin or pterin or on a coordinated-transition-metal cation.<sup>3</sup> However, our crystallographic studies show that RhCC is devoid of any cofactor. The metal ion that is present in RhCC was identified as Mg<sup>2+</sup>; as a redox-inactive metal ion, Mg<sup>2+</sup> cannot facilitate the reaction between 4HPP and molecular oxygen.<sup>35,36</sup> Furthermore, the distance between the Mg<sup>2+</sup> ion and Pro1 in the presumed active site is over 14 Å, which would preclude a direct involvement of Mg<sup>2+</sup> in catalysis. Finally, removal of the Mg<sup>2+</sup> ion upon mutagenesis of its binding site has no significant effect on the oxygenase activity of RhCC. The combination of these observations led us to identify RhCC as a rare example of a cofactor-independent oxygenase.

Scheme 2. Oxygenation of Substrate 4HPP Catalyzed by RhCC<sup>a</sup>

<sup>a</sup>A proposed mechanism for the RhCC-catalyzed oxygenation of 4HPP to yield hydroperoxide 4.

In recent years, a few enzymes have been identified as cofactor-independent oxygenases.<sup>4</sup> The catalytic mechanisms of these enzymes seem to have two features in common, being a general base-catalyzed abstraction of a proton from the substrate, thereby creating a substrate anion, in combination with substrate-assisted catalysis.<sup>4,7,37</sup> Along the reaction pathway, the substrate anion is converted into a radical by single-electron transfer to dioxygen creating a caged “substrate radical–superoxide anion” pair. The ability of the substrate to stabilize the remaining unpaired electron is a determining feature. Because the substrate is able to generate a stable radical, it effectively facilitates the activation of molecular oxygen and acts as a cofactor in the reaction. Via this mechanism, the substrate is initially converted into an organic hydroperoxide, which leads to the formation of the final product or products via subsequent reactions.

These common mechanistic features of cofactor-independent oxygenases can be applied to the RhCC-catalyzed conversion of 4HPP to explain the formation of presumed hydroperoxide intermediate 4 (Scheme 2). We propose that the reaction is initiated by proton abstraction from the 2-hydroxyl group of 4HPP that is mediated by an active-site general base residue; this results in the formation of a carbanion at the C3 carbon of the substrate. Subsequently, the transfer of a single electron from the carbanion to an appropriately positioned dioxygen molecule results in the formation of a triplet-state caged-radical pair, consisting of a superoxide anion and a resonance-stabilized radical cation of 4HPP (Scheme 2, Figure 5). Finally, spin inversion of one of the unpaired electrons of the superoxide anion in the caged-radical pair yields a singlet state that allows C–O bond formation between 4HPP and molecular oxygen to take place, yielding hydroperoxide 4 as the initial product.

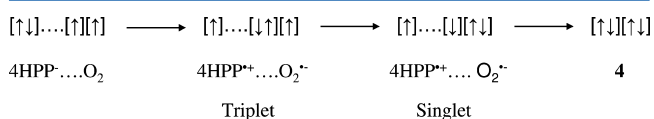


**Figure 5.** Diagram showing (i) the spin states of the valence electrons that initially form the lone electron pair at the carbon atom of 4HPP<sup>−</sup> that bears the negative charge and (ii) both unpaired electrons of dioxygen during the course of the proposed mechanism.<sup>5</sup> Transfer of a single electron from the lone pair at the anionic position of 4HPP<sup>−</sup> to dioxygen yields a triplet-state caged-radical pair. Subsequently, one of the electrons of the superoxide anion in the caged-radical pair undergoes spin inversion, which is a crucial step in the reaction mechanism, causing the caged-radical pair to be converted into the singlet state. The two remaining unpaired electrons in the singlet-state caged-radical pair now have opposite spin signs, which allows them to form readily a set of paired electrons. This results in C–O bond formation, yielding 4 as the initial product of the enzymatic oxygenation reaction.

Further support for this mechanism comes from activity assays with substrate analogue phenylenolpyruvate (9) (Supporting Information Chart 1). Although the 2-hydroxyl group of 9 could be deprotonated, the lack of a *p*-hydroxyl substituent on the ring makes this compound less suitable for stabilizing a radical cation that would be formed upon single-electron transfer from the substrate anion to dioxygen. Hence, 9 appears to be an interesting probe to investigate the requirement of substrate-assisted catalysis in the reaction mechanism. As anticipated, RhCC was found not to accept 9 as substrate, which is fully consistent with the proposed mechanism shown in Scheme 2.

In summary, we provide evidence for cofactor-independent oxygenation of 4HPP within a protein architecture (i.e., the  $\beta$ – $\alpha$ – $\beta$  fold) that is generally employed to catalyze tautomerization, dehalogenation, or decarboxylation reactions. Unfortunately, the genomic context of the gene encoding RhCC does not provide any clues about the biological function of this protein in *R. jostii* RHA1 because the gene coding for RhCC is flanked by genes encoding hypothetical proteins annotated as proteins similar to either enoyl CoA hydratase or an  $\alpha/\beta$  hydrolase fold. In the absence of a pathway context, it is tempting to speculate that the oxidative cleavage of 4HPP to yield products 2 and 3 might be the true physiological function of RhCC. However, although the  $\beta$ – $\alpha$ – $\beta$  fold is used here to host oxygen chemistry, which is proposed to involve hydroperoxide intermediate 4, it clearly lacks the ability to direct the sensitive chemistry of this highly reactive intermediate to prevent the formation of additional products. Indeed, RhCC could be an accidental oxygenase that is able to activate 4HPP by deprotonation of its 2-hydroxyl group but that prevents formation of the keto form of the substrate, allowing the 4HPP anion to react with a correctly positioned O<sub>2</sub> molecule. Therefore, the question remains as to whether the oxygenase activity of RhCC is physiologically relevant or reflects catalytic promiscuity.<sup>38,39</sup> Nonetheless, this work sets the stage for in-depth mechanistic and structural studies of RhCC that could identify the residues involved in catalysis as well as the additional features necessary for a highly specific cofactor-independent oxygenase. Work is in progress to determine the crystal structure of RhCC in complex with 4HPP or a 4HPP analog that cannot be converted by RhCC (i.e., 9 or (*E*)-2-fluoro-*p*-hydroxycinnamic acid (10, Supporting Information Chart 1)).

## ■ ASSOCIATED CONTENT

### Supporting Information

Figures, tables, <sup>18</sup>O-incorporation results, spectroscopic data, and discussion of <sup>18</sup>O-incorporation data. This material is available free of charge via the Internet at <http://pubs.acs.org>.

## AUTHOR INFORMATION

### Corresponding Author

\*Phone: +31-50-3633354. Fax: +31-50-3633000. E-mail: g.j.poelarends@rug.nl.

### Funding

This research was financially supported by The Netherlands Organisation for Scientific Research (VIDI grant 700.56.42) and the European Research Council under the European Community's Seventh Framework Programme (FP7/2007-2013)/ERC grant agreement no. 242293 to G.J.P.

### Notes

The authors declare no competing financial interest.

## ACKNOWLEDGMENTS

We thank the staff of the ESRF (Grenoble) for providing facilities for diffraction measurements and for assistance. We thank C.M. Jeronimus-Stratingh and A. van Dam for their expert assistance in acquiring and interpreting the ESI-MS spectra, Dr. R. van der Geize for the kind gift of genomic DNA of *R. jostii* RHA1, and Prof. Dr. C.P. Whitman for the kind gift of (*E*)-2-fluoro-*p*-hydroxycinnamic acid and for critically reading the manuscript.

## REFERENCES

- (1) Kerr, R. A. (2005) The story of O<sub>2</sub>. *Science* 308, 1730–1732.
- (2) Klinman, J. P. (2007) How do enzymes activate oxygen without inactivating themselves? *Acc. Chem. Res.* 40, 325–333.
- (3) Bugg, T. D. H. (2003) Dioxygenase enzymes: catalytic mechanisms and chemical models. *Tetrahedron* 59, 7075–7101.
- (4) Fetzner, S., and Steiner, R. S. (2010) Cofactor-independent oxidases and oxygenases. *Appl. Microbiol. Biotechnol.* 86, 791–804.
- (5) Minaev, B. F., and Minaeva, V. A. (2008) Spin-dependent binding of dioxygen to heme and charge-transfer mechanism of spin-orbit coupling enhancement. *Ukr. Bioorg. Acta* 2, 56–64.
- (6) Allen, R. C. (1994) Role of oxygen in phagocyte microbicidal action. *Environ. Health Perspect. Suppl.* 102 (Suppl. 10), 201–208.
- (7) Tseng, C. C., Vaillancourt, F. H., Bruner, S. D., and Walsh, C. T. (2004) DpgC is a metal- and cofactor-free 3,5-dihydroxyphenylacetyl-CoA 1,2-dioxygenase in the vancomycin biosynthetic pathway. *Chem. Biol.* 11, 1195–1203.
- (8) Thierbach, S., Bui, N., Zapp, J., Chhabra, S. R., Kappl, R., and Fetzner, S. (2014) Substrate-assisted O<sub>2</sub> activation in a cofactor-independent dioxygenase. *Chem. Biol.* 21, 217–225.
- (9) Bugg, T. D. H. (2014) How to break the rules of dioxygen activation. *Chem. Biol.* 21, 168–169.
- (10) Steiner, R. A., Janssen, H. J., Roversi, P., Oakley, A. J., and Fetzner, S. (2010) Structural basis for cofactor-independent dioxygenation of *N*-heteroatomic compounds at the  $\alpha/\beta$ -hydrolase fold. *Proc. Natl. Acad. Sci. U.S.A.* 107, 657–662.
- (11) Whitman, C. P. (2002) The 4-oxalocrotonate tautomerase family of enzymes: how nature makes new enzymes using a beta-alpha-beta structural motif. *Arch. Biochem. Biophys.* 402, 1–13.
- (12) Poelarends, G. J., and Whitman, C. P. (2004) Evolution of enzymatic activity in the tautomerase superfamily: mechanistic and structural studies of the 1,3-dichloropropene catabolic enzymes. *Bioorg. Chem.* 32, 376–392.
- (13) Poelarends, G. J., Puthan Veetil, V., and Whitman, C. P. (2008) The chemical versatility of the beta-alpha-beta fold: catalytic promiscuity and divergent evolution in the tautomerase superfamily. *Cell. Mol. Life Sci.* 65, 3606–3618.
- (14) Wasiel, A. A., Rozeboom, H. J., Hauke, D., Baas, J. B., Zandvoort, E., Quax, W. J., Thunnissen, A.-M. W. H., and Poelarends, G. J. (2010) Structural and functional characterization of a macrophage migration inhibitory factor homologue from the marine cyanobacterium *Prochlorococcus marinus*. *Biochemistry* 49, 7572–7581.
- (15) Sambrook, J., Fritsch, E. F., and Maniatis, T. (1989) *Molecular Cloning: A Laboratory Manual*, 2nd ed., Cold Spring Harbor Laboratory, Cold Spring Harbor, NY.
- (16) Waddell, W. J. (1956) A simple ultraviolet spectrophotometric method for the determination of protein. *J. Lab. Clin. Med.* 48, 311–314.
- (17) Batty, T. G., Kontogiannis, L., Johnson, O., Powell, H. R., and Leslie, A. G. (2011) iMOSFLM: A new graphical interface for diffraction-image processing with MOSFLM. *Acta Crystallogr., Sect. D* 67, 271–281.
- (18) Evans, P. R., and Murshudov, G. N. (2013) How good are my data and what is the resolution? *Acta Crystallogr., Sect. D* 69, 1204–1214.
- (19) Collaborative Computational Project, Number 4. (1994) The CCP4 suite: Programs for protein crystallography. *Acta Crystallogr., Sect. D* 50, 760–763.
- (20) McCoy, A. J., Grosse-Kunstleve, R. W., Adams, P. D., Winn, M. D., Storoni, L. C., and Read, R. J. (2007) Phaser crystallographic software. *J. Appl. Crystallogr.* 40, 658–674.
- (21) Adams, P. D., Afonine, P. V., Bunkoczi, G., Chen, V. B., Davis, I. W., Echols, N., Headd, J. J., Hung, L. W., Kapral, G. J., Grosse-Kunstleve, R. W., McCoy, A. J., Moriarty, N. W., Oeffner, R., Read, R. J., Richardson, D. C., Terwilliger, T. C., and Zwart, P. H. (2010) PHENIX: A comprehensive Python-based system for macromolecular structure solution. *Acta Crystallogr., Sect. D* 66, 213–221.
- (22) Kabsch, W. (2010) Integration, scaling, space-group assignment and post-refinement. *Acta Crystallogr., Sect. D* 66, 133–144.
- (23) Chen, V. B., Arendall, W. B., III, Headd, J. J., Keedy, D. A., Immormino, R. M., Kapral, G. J., Murray, L. W., Richardson, J. S., and Richardson, D. C. (2010) MolProbity: All-atom structure validation for macromolecular crystallography. *Acta Crystallogr., Sect. D* 66, 12–21.
- (24) Krissinel, E., and Henrick, K. (2004) Secondary-structure matching (SSM), a new tool for fast protein structure alignment in three dimensions. *Acta Crystallogr., Sect. D* 60, 2256–2268.
- (25) Waterhouse, A. M., Procter, J. B., Martin, D. M., Clamp, M., and Barton, G. J. (2009) Jalview version 2—a multiple sequence alignment editor and analysis workbench. *Bioinformatics* 25, 1189–1191.
- (26) Zheng, H., Chordia, M. D., Cooper, D. R., Chruszcz, M., Müller, P., Sheldrick, G. M., and Minor, W. (2014) Validation of metal-binding sites in macromolecular structures with the CheckMyMetal web server. *Nat. Protoc.* 9, 156–170.
- (27) Poelarends, G. J., Serrano, H., Person, M. D., Johnson, W. H., Jr., Murzin, A. G., and Whitman, C. P. (2004) Cloning, expression, and characterization of a *cis*-3-chloroacrylic acid dehalogenase: Insights into the mechanistic, structural, and evolutionary relationship between isomer-specific 3-chloroacrylic acid dehalogenases. *Biochemistry* 43, 759–772.
- (28) Poelarends, G. J., Serrano, H., Person, M. D., Johnson, W. H., Jr., and Whitman, C. P. (2008) Characterization of Cg10062 from *Corynebacterium glutamicum*: implications for the evolution of *cis*-3-chloroacrylic acid dehalogenase activity in the tautomerase superfamily. *Biochemistry* 47, 8139–8147.
- (29) Baas, B. J., Zandvoort, E., Wasiel, A. A., Quax, W. J., and Poelarends, G. J. (2011) Characterization of a newly identified mycobacterial tautomerase with promiscuous dehalogenase and hydratase activities reveals a functional link to a recently diverged *cis*-3-chloroacrylic acid dehalogenase. *Biochemistry* 50, 2889–2899.
- (30) De Jong, R. M., Bazzacco, P., Poelarends, G. J., Johnson, W. H., Jr., Kim, Y. J., Burks, E. A., Serrano, H., Thunnissen, A. M. W. H., Whitman, C. P., and Dijkstra, B. W. (2007) Crystal structures of native and inactivated *cis*-3-chloroacrylic acid dehalogenase. Structural basis for substrate specificity and inactivation by (R)-oxirane-2-carboxylate. *J. Biol. Chem.* 282, 2440–2449.
- (31) Guo, Y., Serrano, H., Johnson, W. H., Jr., Ernst, S., Hackert, M. L., and Whitman, C. P. (2011) Crystal structures of native and inactivated *cis*-3-chloroacrylic acid dehalogenase: Implications for the catalytic and inactivation mechanisms. *Bioorg. Chem.* 39, 1–9.

- (32) Lubetski, J. B., Swope, M., Dealwis, C., Blake, P., and Lolis, E. (1999) Pro-1 of macrophage migration inhibitory factor functions as a catalytic base in the phenylpyruvate tautomerase activity. *Biochemistry* 38, 7346–7354.
- (33) Jefford, C. W., Knöpfel, W., and Cadby, P. A. (1978) Oxygenation of 3-aryl-2-hydroxyacrylic acids. The question of linear fragmentation vs. cyclization and cleavage of intermediates. *J. Am. Chem. Soc.* 100, 6432–6436.
- (34) Oyama, S. T. (2008) Rates, Kinetics, and Mechanisms of Epoxidation: Homogeneous, Heterogeneous, and Biological Routes, in *Mechanisms in Homogeneous and Heterogeneous Epoxidation Catalysis* (Oyama, S. T., Ed.) pp 3–100, Elsevier, Amsterdam, The Netherlands.
- (35) Tsui, E. Y., Tran, R., Yano, J., and Agapie, T. (2013) Redox-inactive metals modulate the reduction potential in heterometallic manganese-oxido clusters. *Nat. Chem.* 5, 293–299.
- (36) Kriech, S., Yu, L., Reiher, M., and Westerhausen, M. (2010) Subvalent organometallic compounds of the alkaline earth metals in low oxidation states. *Eur. J. Inorg. Chem.*, 197–216.
- (37) Widboom, P. F., Fielding, E. N., Liu, Y., and Bruner, S. D. (2007) Structural basis for cofactor-independent dioxygenation in vancomycin biosynthesis. *Nature* 447, 342–345.
- (38) Baas, B. J., Zandvoort, E., Geertsema, E. M., and Poelarends, G. J. (2013) Recent advances in the study of enzyme promiscuity in the tautomerase superfamily. *ChemBioChem.* 14, 917–926.
- (39) Copley, S. D. (2003) Enzymes with extra talents: moonlighting functions and catalytic promiscuity. *Curr. Opin. Chem. Biol.* 7, 265–272.